PHYSICAL REVIEW A VOLUME 27, NUMBER 2 FEBRUARY 1983

Observation of ${}^1P$-${}^1D$, ${}^1P$-${}^{1,3}F$, and ${}^1P$-${}^{1,3}H$ motional Stark-effect-induced anticrossings in ^{4}He: Determination of zero-field level separations

H. Le, M. Rosenbluh,* and B. Lax
Francis Bitter National Magnet Laboratory, MIT, Cambridge, Massachusetts 02139

Terry A. Miller†
Bell Laboratories, Murray Hill, New Jersey 07974

(Received 20 November 1981; revised manuscript received 2 September 1982)

Anticrossings induced by the motional Stark effect created by atoms moving perpendicular to a strong magnetic field have been observed in ^{4}He. These anticrossings couple the $n\,{}^1P$ state with the nominal $n\,{}^1D$, $n\,{}^1F$, $n\,{}^3F$, and $n\,{}^{1,3}$H states via first-order (for the ${}^1D$) and second-order Stark effects. The theory is derived to explain the line shape in the second-order case. This theory, along with the previously existing first-order-effect line-shape theory, is used to obtain the zero-velocity crossing points. These values are used in a least-squares fit to determine the zero-field intervals. The $n\,{}^1P-{}^1D_2$ interval is determined precisely for $n=6$, 7, and 8 and the $n\,{}^1G-nH_{\text{av}}$ interval is determined for $n=6$ and 7. A power-series expansion establishes the $n\,{}^1P$ energy levels with respect to the higher nL states with high precision.

I. INTRODUCTION

Recently, advanced experimental techniques have allowed spectroscopic studies of the helium atom with a many-fold improvement in precision over the classical optical measurements.[1-4] This progress has created new theoretical interest in the pentultimately simplest atom He. In particular, the development of the parametrized series expansion of energy intervals in odd powers of the principal quantum number n has proved quite useful.[5] The series expansion predicts the energy interval between any two states once the coefficients, which depend only on spin, orbital, and total angular momentum, are known. These coefficients can be phenomenologically determined from empirical data. While measurements of energy intervals between high angular momentum states ($L\geq 2$) are becoming more abundant, the high-precision data on the intervals between low L (S, P, and D) states is still quite sparse. In this paper, we present measurements of some of these intervals.

The electric-field-induced anticrossing technique has previously been applied to spectroscopic measurements of helium.[3] For an atomic gas in a magnetic field, an electric field is provided by the well-known motional Stark effect (MSE), and if the gas is in thermal equilibrium, the electric field, although inhomogeneous, can be accurately inferred from the known kinetic theory of a gas.[2] Anticrossings resulting from the MSE in hydrogen have been known for quite some time[6] and in fact, the basic treatment of the theory of anticrossing signals[7] arose partially in regard to this observation. More recently, this effect has been observed with He atoms, and it is referred to as a MSE-induced anticrossing.[8]

The observations reported here fall into two general categories. The first category consists of anticrossings between the $n\,{}^1P$ and $n\,{}^3D$ states for $n=7$ and 8. These anticrossings are characterized by the nominal selection rule on the magnetic quantum numbers of $|\Delta M_L|=0$ and $|\Delta M_S|=1$. Such an anticrossing is possible because of the existence of two relevant perturbations as is shown schematically in Fig. 1(a). The $n\,{}^1D$ levels provide an intermediate state, the magnetic spin-orbit operator $\hat{H}_{\text{FS}}$ mixes the $n\,{}^1D$ and ${}^3D$ states, while the MSE operator mixes the $n\,{}^1D$ and $n\,{}^1P$ states. The pairs of Zeeman levels actually coupled are indicated in Fig. 1(a).

The second category of observation pertains to anticrossings between $n\,{}^1P$ and ${}^{1,3}F$ and ${}^{1,3}H$ states. In the ${}^{1,3}F$ and ${}^{1,3}H$ states the spin-orbit mixing discussed above is sufficiently large that singlet and triplet quantum numbers are not very meaningful, and for the purposes of our experiment it is best to simply refer to a mixed level, e.g., ${}^{1,3}F$ or ${}^{1,3}H$. Figure 1(b) illustrates the mechanism[9] giving rise to the ${}^1P$-${}^{1,3}F$ anticrossings. In this case the ${}^1D$ state again plays the role of an intermediate; however, now the

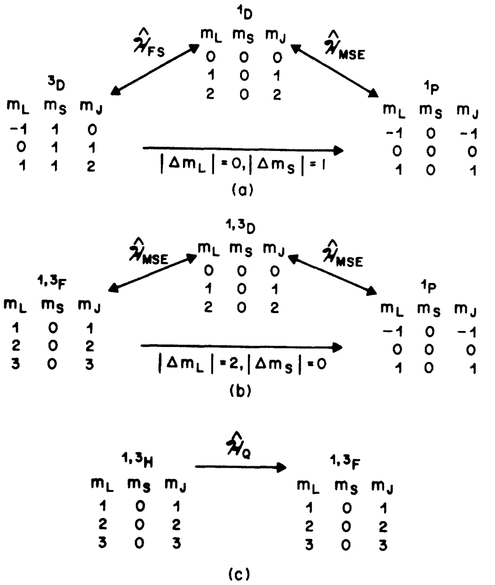

FIG. 1. Mechanisms and selection rules for each class of anticrossing. (a) shows the anticrossing of ^3D states to ^1P via ^1D; $\hat{H}_{\rm FS}$ is the fine-structure Hamiltonian that couples ^3D to ^1D, conserving only m_J, and the MSE Hamiltonian $\hat{H}_{\rm MSE}$ couples ^1D to ^1P with the usual dipole selection rule. (b) shows the $^{1,3}F$-^1P anticrossing via second-order $\hat{H}_{\rm MSE}$ coupling. Although the intermediate level is shown simply as $^{1,3}D$ it should be interpreted as the $^{1,3}D$ character in all the high L states. The eigenvectors appropriate at a given field were used for actual calculation. ^3F-^1F mixing is implicitly assumed. (c) shows the mixing of F and H character by the quadratic Zeeman term $\hat{H}_Q$ thereby allowing for the $^{1,3}H$ states the same anticrossings as experienced by $^{1,3}F$ states.

coupling of the ^1D level to both the $^{1,3}F$ and the ^1P is via the MSE operator $\hat{H}_{\rm MSE}$. Again the details of the M_L and M_S selection rules are shown in Fig. 2(b). Figure 3(c) shows that the $^{1,3}F$ and $^{1,3}H$ states are coupled by the quadratic Zeeman Hamiltonian $\hat{H}_Q$. At the fields employed in these experiments, the H_Q coupling of the F and H states is sufficiently strong so that ^1P-$^{1,3}H$ anticrossings, induced by the same second-order MSE, are easily observed.

As can be seen from Fig. 1 various magnetic sublevels of the nP state can anticross with corresponding magnetic sublevels of the $n\,^3D$, ^1F, ^3F, ^1H, and ^3H states. The selection rules governing the 15 possible magnetically tunable anticrossings are shown in Fig. 1. Since the ^1P to ^1H and ^3H anticrossings are not experimentally resolved, this reduces the number of observable anticrossings to 12. All 12 of these anticrossings were indeed observed. However, two,

$$^1P(m_L=-1,m_S=0)-{}^3D(m_L=-1,m_S=1)$$

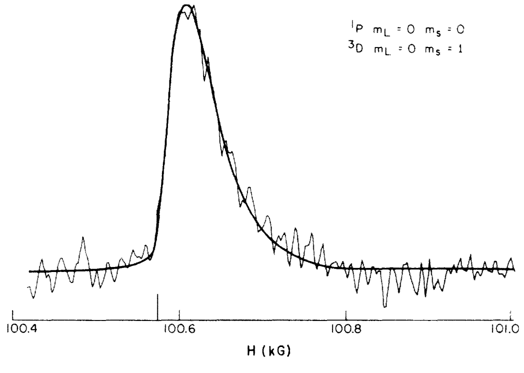

FIG. 2. Trace of the ^1P-^3D anticrossing with the nominal magnetic quantum numbers as indicated. The experimental conditions are 15 mTorr He pressure, 3 mA electron current, and 10 min averaging time.

and

$$^1P(m_L=1,m_S=0)-{}^3D(m_L=1,m_S=1)\ ,$$

were not analyzed in detail because their widths were relatively great, and therefore the corresponding uncertainties associated with the measurement of their line centers were large. The inclusion of them in the final data analysis would not improve the determination of the zero-field ^1P-^3D separation.

There are a number of imaginable anticrossings involving the ^1P state with other $^{1,3}L$ states which are not included in Fig. 1 and were observed to be

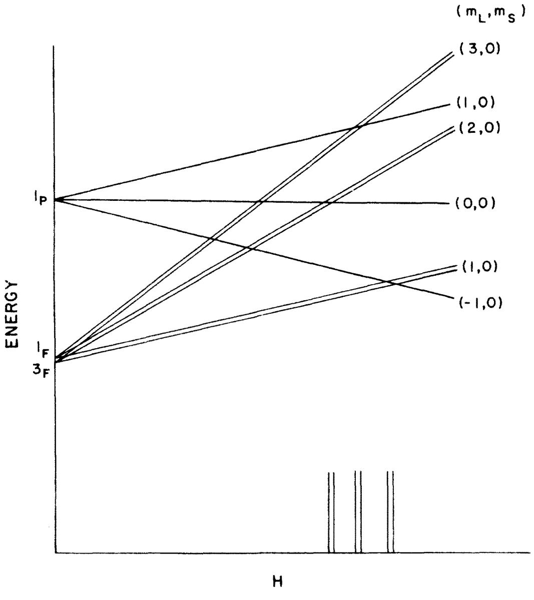

FIG. 3. Energy-level diagram depicting ^1P-$^{1,3}F$ anticrossing. Note that nonlinear Zeeman effects lead to three distinct anticrossings for the ^1P M_L values of 1, 0, and -1, while the singlet-triplet structure of the F state leads to a doubling of each of these anticrossings.

very weak or undetectable. In each case the vanishing or near-vanishing strengths are readily explicable. Anticrossings to states of high even L, i.e., G and I, would require either a coupling of third order or higher by $\hat{H}_{\text{MSE}}$ or mixing by $\hat{H}_Q$ of $^{1,3}D$ character into these high L states. Calculations indicate that neither of these mechanisms is sufficiently strong to give rise to observable anticrossings.

The only remaining states are the $n=8\,^{1,3}K$ levels. Anticrossings from the ^1P to the $^{1,3}K$ states are allowed by mixing via H_Q, as shown in Fig. 1(c), of the K and H and F states. These anticrossings were observed but with limited signal-to-noise (S/N) ratio. Moreover, the mixing by H_Q of 8 H and K is so strong that it is difficult to derive separate zero-field energy positions for these states. An initial appraisal indicated little expectation of significant improvement over the previous $8^{1,3}K$-level determination[3] from the available data and so the ^1P-$^{1,3}K$ anticrossing analysis was not pursued, nor are unique values for the ^1P-$^{1,3}H$ separation reported.

Assuming a Zeeman tuning theory is available so that the positions where levels would cross in the absence of coupling can be determined, one can use the observed anticrossing positions to determine the zero-field energy of the ^1P state with respect to the well-known energy manifold of $^{1,3}D$-F-G states. With less precision, the $^{1,3}H$ states (H_{av}) can also be placed with respect to the $^{1,3}D$-F-G states. The remainder of this paper is divided as follows: Sec. II briefly describes our experimental apparatus, the scheme of analysis is presented in Sec. III, and discussion of the results follows in Sec. IV.

II. EXPERIMENT

The He atoms are excited by a controlled beam of electrons (~90 eV). The relevant states $n\,^{1,3}F,H$ and $n\,^1P$ are not monitored directly but instead via the emission line of the $n\,^3D$-2^3P transition. The anticrossing signals are detected as a change in fluorescence intensity as a function of magnetic field. The experiments were conducted at the lowest practical pressure (< 15 mTorr) and electron current less than 3 mA to avoid stray electric field from space charge. Details of the apparatus can be found elsewhere.[2,8] The magnetic tuning was accomplished with a highly homogeneous 145-kG Bitter magnet.

III. ANALYSIS

As mentioned in the Introduction, there are two categories of anticrossings: (i) ^1P-^3D anticrossings and (ii) ^1P-$^{1,3}F$, $^{1,3}H$ anticrossings. Anticrossings of category (i) are essentially the same in structure and line shape as the ^3D-^3F MSE anticrossings that we discussed previously.[8] An example of such an anticrossing is shown in Fig. 2. The second category (ii) of anticrossings is somewhat more complicated in structure and line shape. Figure 3 shows an energy-level diagram illustrating this type of anticrossing. Figure 4 shows a broad magnetic field scan showing both the $n=6$ ^1P-$^{1,3}F$ and ^1P-$^{1,3}H$ anticrossings. Figures 5 and 6 show higher resolution scans of these anticrossings. The anticrossings in $n=7$ and 8 are quite similar in form to those of $n=6$.

The form of the anticrossings shown in high resolution in Figs. 5 and 6 can be understood by reference to Fig. 3. Each value of m_L for the ^1P state can undergo an anticrossing with a level m_L+2 of the $^{1,3}F$ state. If only the linear Zeeman tuning were considered, these anticrossings would occur at the same magnetic field position; however, diamagnetic Zeeman effects raise this position degeneracy and give rise to three distinct anticrossings. As Fig. 5 indicates, each of these components shows a partially resolved doublet structure. This doublet structure, as exaggerated in Fig. 3, arises from the two F states. The comparable widths and intensities of these doublets are consistent with the strong mixing expected between the nominal ^1F and ^3F levels.

In order to obtain zero-field separations, two steps of analysis must be performed on signals such as are shown in Figs. 2, 5, and 6. First, the line shape must be understood to obtain the "true" crossing point in the absence of perturbation. Second, the magnetic and fine-structure Hamiltonian must be understood to derive from the crossing fields the zero-field separations. In the final analysis these two steps must be done iteratively to ensure consistency.

A. Line shapes

We base our line-shape analysis on our previous treatment[8] of MSE-induced anticrossings. We saw

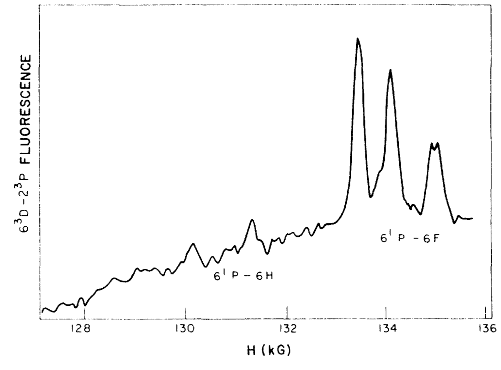

FIG. 4. Broad magnetic-field scan showing $n=6$, ^1P-H_{av} and $n=6$, ^1P-$^{1,3}F$ anticrossings.

in that work that the overall line shape $I(H)$ can be generally represented as

$$I(H)=\int_{-\infty}^{\infty} I_h(H-H')I_i(H'-H_0)dH' \ , \tag{1}$$

where $I_i(H'-H_0)$ is the probability distribution (in this case velocity dependent) for having an anticrossing centered at H', $I_h(H-H')$ is the line shape for the anticrossing centered at H', and H_0 is the hypothetical anticrossing position for an atom with $v_\perp=0$. The line shape I_h can be given by the usual formula[10] for levels a and b,

$$I_h(H-H')=\frac{-2\bar{\tau}^{-1}(\rho_a^0\tau_a-\rho_b^0\tau_b)(K_a\tau_a-K_b\tau_b)\,|\,V_{ab}\,|^2}{4\,|\,V_{ab}\,|^2 f_\tau+\hbar^2/\bar{\tau}^2+g_e^2u_0^2(H-H')^2} \ , \tag{2}$$

where

$$\bar{\tau}^{-1}=\tau_a^{-1}+\tau_b^{-1} \ ,$$

$$f_\tau=\tau_a\tau_b/\bar{\tau}^2 \ ,$$

and $u_0g_e=\partial E/\partial H$ with E being an exact expression for the energy difference between the two levels a and b as a function of magnetic field, neglecting the contributions from V_{ab}, $K_{a(b)}$ is a constant proportional to the detector sensitivity to radiation from levels $a(b)$, and the remaining symbols have their usual definitions.[10] The perturbation matrix element V_{ab} is perhaps the most crucial factor appearing in I_h. For the ^1P-^3D case, the terms of the Hamiltonian representing the MSE, $\hat{H}_{\text{MSE}}$, can be written

$$\hat{H}_{\text{MSE}}=E_\perp^2\begin{bmatrix}\alpha'_{PP} & 0\\ 0 & \alpha'_{DD}\end{bmatrix}+E_\perp\begin{bmatrix}0 & \mu_{PD}\\ \mu^*_{PD} & 0\end{bmatrix}$$

$$=\hat{H}^D_{\text{MSE}}+\hat{V}_{PD} \ , \tag{3}$$

thereby defining $\hat{V}_{PD}$ as the off-diagonal part of $\hat{H}_{\text{MSE}}$ and $\hat{H}^D_{\text{MSE}}$ as the diagonal part. The α''s are the relevant polarizabilities (excluding the contributions of the anticrossing states to each other), and μ_{PD} represents the dipole moment between the P and D states. The MSE electric field $E_\perp$ is given by

$$E_\perp=v_\perp H/c \ . \tag{4}$$

In the case of the ^1P-$^{1,3}F$ or $^{1,3}H$ anticrossings first-order perturbation theory gives a vanishing coupling between the relevant states, and one must turn to second-order Rayleigh-Schrödinger[11] perturbation theory (a Van Vleck transformation). In this approximation we have

$$\hat{H}_{\text{MSE}}=E_\perp^2\begin{bmatrix}\alpha_{PP} & 0\\ 0 & \alpha_{FF(HH)}\end{bmatrix}+E_\perp^2\begin{bmatrix}0 & \alpha_{PF(H)}\\ \alpha^*_{PF(H)} & 0\end{bmatrix}$$

$$=\hat{H}^D_{\text{MSE}}+\hat{V}_{PF}(H) \ , \tag{5}$$

where α_{ii} is the total polarizability of the i state is the coefficient of the electric field coupling between the i and j states. We note that in categories (i) and (ii) $\hat{H}^D_{\text{MSE}}$ is of the same form, while $\hat{V}_{ab}$ differs for the two cases.

The form of the distribution function I_i depends only upon $\hat{H}^D_{\text{MSE}}$, and thus is the same as was previously given,[8]

$$I_i(H'-H_0)=\begin{cases}\dfrac{2\pi c^2 g_e\mu_0}{|\,\alpha\,|H_0^2v_0^2}\exp[-c^2g_e\mu_0 2\pi(H'-H_0)\alpha H_0^2v_0^2] \ , & \dfrac{H'-H_0}{\alpha}\geq 0\\ 0 \ , \quad \dfrac{H'-H_0}{\alpha}<0 & \end{cases} \tag{6}$$

where α without subscripts is defined as the difference in the diagonal matrix elements of $\hat{H}^D_{\text{MSE}}$.

If we insert the definition of V_{ab} for the ^1P-^3D case into Eq. (2) and use Eqs. (1) and (6), we obtain the complete line-shape formula,

$$I(H)=|B|\int_{H_0}^{\pm\infty}\frac{A(H'-H_0)e^{-B(H'-H_0)dH'}}{2Af_\tau(H'-H_0)+\hbar^2\tau^{-2}+g_e^3\mu_0^2(H-H')^2U^2} \tag{7}$$

with

$$A=4\pi g_e\mu_0\mu_{PD}^2/\alpha\ ,$$

$$B=2\pi c^2 g_e\mu_0/\alpha H_0^2 v_0^2\ ,$$

$$U=1+\left[1-\frac{H^2}{H_0^2}\right]\left[\frac{H'-H_0}{H-H'}\right].$$

In our earlier work, H_0 was assumed to be much greater than $(H-H_0)$ and thus the factor U reduces to unity. In our present work we find that the experimental line shapes are better fit by including the complete form of U. For the case of the ^1P-$^{1,3}F$ for $^{1,3}H$ anticrossings

$$|V_{ab}|^2=\alpha_{ab}^2\frac{H^4v_\perp^4}{c^4}\approx\alpha_{ab}^2H_0^4V_\perp^4/c^4=\left[\frac{2\pi g_e\mu_0\alpha_{ab}}{\alpha}\right]^2(H-H_0)^2\ . \tag{8}$$

Inserting this definition for V_{ab} into Eq. (2) and again using Eqs. (1) and (6) yields

$$I(H)=|B|\int_{H_0}^{\pm\infty}\frac{A(H'-H_0)^2e^{-B(H'-H_0)}dH'}{2Af_\tau(H'-H_0)^2+\hbar^2\tau^{-2}+g_e^2\mu_0^2(H-H')^2U^2} \tag{9}$$

with

$$A=2\left[\frac{2\pi g_e\mu_0\alpha_{ab}}{\alpha}\right]^2$$

and B and U as before.

In our derivation of the anticrossing mechanism, we approximate an infinite dimensional system by a two-level one. The criterion for validity of this approximation is a large energy separation of these two levels from the rest and/or a small coupling of these states to others. Thus the perturbation matrix has an error of the order of $V^2/(\Delta E)^2$, where V represents the perturbation coupling to other states and ΔE the energy separation. (This is the next term in the series of Rayleigh-Schrödinger perturbation theory.) This criterion is not perfectly met in the ^1P-$^{1,3}F$ and ^1P-$^{1,3}H$ anticrossings observed here, since ^1F and ^3F are close to each other, and certainly the higher-order terms of interaction are not entirely negligible.

In particular, the mixing of the singlet and triplet F levels creates nonzero, electric field, off-diagonal matrix elements between all three states, ^1P, ^1F, and ^3F. The rigorous approach to the problem is the construction of a three-level Hamiltonian; however, its analytic complexity and the minimal effect these corrections have on our experimental data lead us to avoid this approach. We did, however, slightly modify the polarizabilities α_{FF} in Eq. (5) by taking into account these other off-diagonal matrix elements. These modifications lead to a slight, but clear improvement in the agreement between theory and experiment without introducing any new variables. The details of the calculations are given in Ref. 12.

The anticrossing of the ^1P and H states is governed by the same mechanism, differing only in the actual matrix elements. The quadratic Zeeman term mixes states with $|\Delta L|=2$ and the F state is sufficiently close to the H state that the mixing is almost exclusively between the F and H states. (This can be contrasted to, for example, D and G states where the mixing is relatively much smaller.) In this case, the interaction is strong enough to give ^1P-H anticrossing widths that are comparable to those of the ^1P-F anticrossings.

The ^1P-^3D anticrossings are much simpler in nature and their treatment needs no further modifications, since they adequately meet the two-level model specification.

B. Extrapolation to zero-field intervals

The objective of our analysis is the determination of the zero-field energy intervals. This is accomplished by a least-squares fitting of the H_0's obtained from the preceding line-shape analysis. Since some of the parameters of the line-shape analysis de-

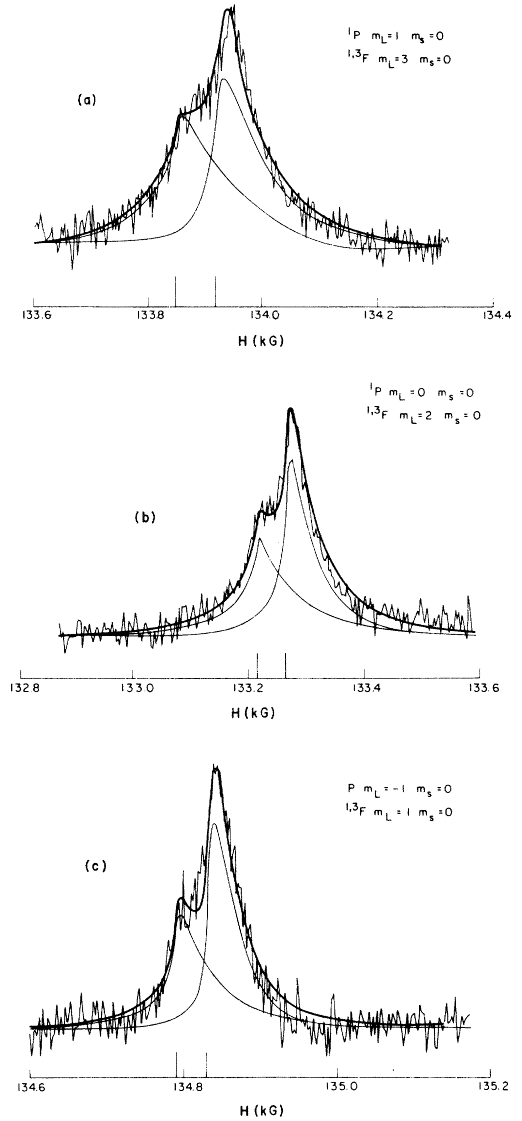

FIG. 5. High-resolution scan of 6^1P-$^{1,3}F$ anticrossings. Traces a,b,c correspond to the anticrossings for the ^1PM_L values of 1, 0, and -1, respectively. The light solid lines depict computer simulation of the positions of the individual ^1F and ^3F anticrossings. The heavier solid lines, matching the experimental data, are the composite of the ^1F and ^3F simulations.

pend on the values of these zero-field intervals (especially for the P-H anticrossings), the process must be performed iteratively. Optical data[13] serve as reasonable initial estimates for the intervals, and thus one or two iterations are sufficient for all the lines.

We begin by describing our calculation of the Zeeman tuning. The Hamiltonian of a helium atom in a magnetic field can be expressed as

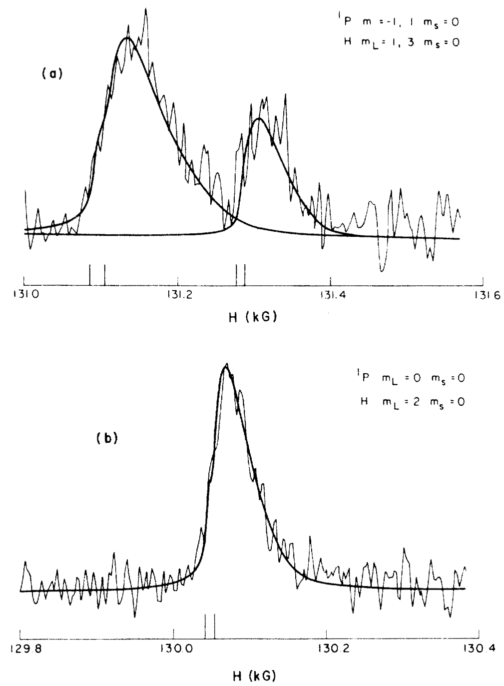

FIG. 6. High-resolution scan of 6^1P-H_{av} anticrossing. Traces a and b correspond to the anticrossings for the ^1PM_L values of ±1 and 0, respectively. The solid lines are computer simulations of the line shapes. The singlet-triplet structure of the H state is not observed experimentally.

$$\hat{H}_{\mathrm{mag}}=\hat{H}_0+\hat{H}_z+\hat{H}_Q\ , \tag{10}$$

where $\hat{H}_0$ is the zero-field Hamiltonian and $\hat{H}_z$ and $\hat{H}_Q$ are, respectively, the linear and diamagnetic Zeeman terms. $\hat{H}_0$ is assumed to include all the electrostatic effects giving rise to the zero-field eigenvalues characterized by the quantum numbers L, S, and J.

The Zeeman levels are obtained by diagonalization of $\hat{H}$ within a basis consisting of all states with the same quantum number n and parity. The radial part of the wave function is hydrogenic

$$R_{nl}^{Z=1}(r_2)R_{10}^{Z=2}(r_1)$$

and diagonal matrix elements are corrected by substituting for n, $n^*=n-\delta_{L,S}$, where $\delta_{L,S}$ is the quantum defect.[10,14,15] For off-diagonal matrix elements it has been shown[12] that if one uses

$$n_{l_1,l_2}^*=(n_{l_1}^*n_{l_2}^*)^{1/2}\ ,$$

sufficient accuracy is obtained. The spherical part of the wave function is taken as

$$Y_1^{m_1}(\hat{r}_2)Y_0^0(\hat{r}_1\,|\,SM_s\rangle\ ,$$

i.e., the Paschen-Bach limit. In this basis, the matrix elements of $\hat{H}_z$ and $\hat{H}_Q$ assume simple expressions as the expectation values of spherical tensors of rank 0 through 2. However, for $\hat{H}_0$, the more natural basis vectors are

$$\cos\theta_L \mid (L,S=1)JM_J\rangle + \sin\theta_L \mid (L,S=0)JM_J\rangle \ ,$$
$$-\sin\theta_L \mid (L,S=1)JM_J\rangle + \cos\theta_L \mid (L,S=0)JM_J\rangle \ , \tag{11}$$

which express the mixing of $J=L$ states with different spin. θ_L is the single parameter, depending only on L, that characterizes the singlet-triplet mixing. (Even L is not conserved, but the mixing between L states is completely negligible for our purpose here.) In this basis, $\hat{H}_0$ is diagonal, and its eigenvalues constitute the spectrum of the manifold. The parameters θ_L's are calculated using the α^2 spin-violating terms of the helium Hamiltonian ($\hat{H}_3$ and $\hat{H}_5$ of Breit-Bether notation[16]).

The nonrelativistic electric exchange effect[17,18] is the major contribution to the singlet-triplet electrostatic splitting. We follow the approach of Cok and Lundeen[18] and define a phenomenological electric exchange quantity X, which will fit the known empirical or extrapolated energy-level separations. We use the X values of Cok and Lundeen[18] and derive θ_L's from the matrix diagonalization. The resulting energy levels fit best the known empirical or extrapolated values. Table I contains the set of values of θ_L used in this analysis.

The diagonal elements of $\hat{H}_0$ thus correspond to the zero-field energy levels. In principle, the anticrossing positions, ^1P-^1F, ^1P-^3F, and ^1P-H_{av} are affected by all the zero-field intervals. However, the sensitivity of an anticrossing position to the various intervals varies widely. The anticrossing positions are only weakly affected by the intervals ^1S-^1P, H_{av}-I_{av}, and I_{av}-K_{av}. We thus fix the ^1S-^1P interval at its optical value[13] and take the H_{av}-I_{av} and I_{av}-K_{av} intervals (where applicable) from the anticrossing results (either direct or extrapolated) of Ref. 3. While neither of these sources is particularly precise, these intervals are known well enough so as to introduce no further uncertainty in our calculated anticrossing positions. We list these values in Table II for reference. Fortunately, there are high-precision measurements[2] for the remaining intervals. These values are listed in Table II also. For $L \geq 4$, singlet and triplet levels are not experimentally resolved, and thus we treat only the average of these states, G_{av}, H_{av}, etc.

This means that the only unknown zero-field intervals are ^1P-^1F and ^1P-H_{av} which are determined by fitting to the observed anticrossings as described below. By using the determined ^1P-^1F and ^1P-H_{av} intervals with the previously known ^1F-$^3G_5$ interval, the interval G_{av}-H_{av} can be deduced, as will be discussed in Sec. IV.

TABLE I. Mixing angle θ_L used in this analysis.

n		θ_L	$\tan\theta_L$
6	$L=3$	0.5440	0.6048
	$L=5$	0.7702	0.9700
7	$L=2$	0.0092	0.0092
	$L=3$	0.5224	0.5758
	$L=5$	0.7702	0.9700
8	$L=2$	0.0090	0.0090
	$L=3$	0.5060	0.5542
	$L=5$	0.7702	0.9700

In the numerical analysis, before $\hat{H}_0$ can be added to $\hat{H}_z$ and $\hat{H}_Q$, the latter must be expressed in the $\hat{H}_0$ eigenfunction basis by a linear transformation. We use the same form for $\hat{H}_z$ and $\hat{H}_Q$ as we have used previously.[2,10] We have estimated the relativistic corrections ($\delta\mu_i$, $i=1$–6 in the notation of Ref. 19) for $\hat{H}_z$ and found them to be no greater than ~ 10 ppm. This corresponds to an effect of a few gauss in our line position. As this is comparable to, or less than, our experimental error, we have not included these effects explicitly in our calculations.

The Zeeman levels and states obtained from the

TABLE II. Constraint intervals used in this analysis in MHz. The values were taken from Ref. 1 except as otherwise noted.

		n	
Intervals	6	7	8
K_{av}-I_{av}			213[a]
I_{av}-H_{av}		490[a]	403[b]
H_{av}-$^1G_4$	c	c	c
$^1G_4$-$^1F_3$	8 854	5 703	3 876
$^1F_3$-$^1D_2$	49 803	31 558	21 226
$^1D_2$-$^1P_1$	c	c	c
$^1P_1$-$^1S_0$	4 797 885[d]	3 003 669[d]	1 997 561[d]
$^1D_2$-$^3D_2^{\mathrm{e}}$	200 946	13 650	9 344
$^3G_4$-$^3F_3^{\mathrm{e}}$	9 007	5 774	3 924
$^3F_3$-$^3D_2^{\mathrm{e}}$	70 523	45 061	30 471
$^3D_2$-$^3P_1^{\mathrm{e}}$	2 016 344[d]	1 269 063[d]	851 686[d]
$^3P_1$-$^3S_1^{\mathrm{e}}$	7 695 015[d]	4 768 157[d]	3 158 338[d]

[a] Reference 3.

[b] Reference 4.

[c] Determined in present analysis, see Table IV.

[d] Reference 13.

[e] The magnetic fine-structure intervals for the triplet states were explicitly included in the calculation. These values are all taken from Ref. 1, except the ^3P intervals which came from Ref. 13.

total matrix diagonalization are used to calculate the line-shape parameters. The fitting procedure thus consists of three steps: (i) calculating H_0 and line-shape parameters, (ii) fitting the data with these parameters and obtaining the experimental values of H_0, $\tilde{H}_0$, and (iii) using $\tilde{H}_0$ in determining the relevant energy intervals, minimizing χ^2, and returning to (i) if unsatisfactory. χ^2 is defined to

$$\chi^2=\sum_i \frac{(\tilde{H}_{0,i}-H_{0,i})^2}{\sigma_1^2}\ . \qquad (12)$$

Thus

$$\frac{\partial\chi^2}{\partial E}=2\sum_i \frac{(\tilde{H}_{0,i}-H_{0,i})}{\sigma_1^2}\frac{\partial H_{0,i}}{\partial E}\ , \qquad (13)$$

where σ_1^2 is the variance of $\tilde{H}_{0,i}$.

IV. DISCUSSION AND RESULTS

A. Line-shape fitting

The above-mentioned step (ii), line fitting, is somewhat involved since there are three parameters for which we do not have precise knowledge: temperature T, lifetime $\bar{\tau}$, and relative populations of the ${}^{1,3}F$ and ${}^{1}P$ states. It turns out that the value of $\bar{\tau}$ within reasonable limits is not critical, and tabulated values[20,21] are adequate. The relative population of singlet and triplet F states is not well determined, so we must adopt a phenomenological relative strength for the singlet and triplet F signals.

TABLE III. Measured field positions, H_0expt, of anticrossing signals. The quoted uncertainty of the measurement is $(\sigma^2+S^2)^{1/2}$ where σ^2 is the variance from the line fit and S is any other experimental uncertainty. The column labeled by H_0calc is the result of a least-squares fitting of the H_0expt values. The values of the zero-field intervals determined by this fit are given in Table IV while the interval values given in Table II were held fixed.

n	P	m_L	m_S	L	m_L	m_S	H_0expt. (kG)	H_0calc (kG)	H_0calc$-H_0$expt. (G)
6									
		-1	0	${}^1F$	1	0	134.793±0.0085	134.787	-6
				${}^3F$	1	0	134.830	134.823	-7
		0	0	${}^1F$	2	0	133.215	133.217	$+2$
				${}^3F$	2	0	133.266	133.271	$+5$
		1	0	${}^1F$	3	0	133.852	133.853	$+1$
				${}^3F$	3	0	133.923	133.926	$+3$
		-1	0	H	1	0	131.286±0.012	133.292	$+6$
		0	0	H	2	0	130.051	130.051	0
		1	0	H	3	0	131.102	131.096	-6
7									
		0	0	${}^3D$	0	1	100.573±0.011	100.575	$+2$
		-1	0	${}^1F$	1	0	85.540±0.010	85.523	-17
				${}^3F$	1	0	85.559	85.547	-12
		0	0	${}^1F$	2	0	84.313	84.324	11
				${}^3F$	2	0	84.348	84.358	10
		1	0	${}^1F$	3	0	84.766	84.769	3
				${}^3F$	3	0	84.811	84.816	5
		-1	0	H	1	0	83.160±0.016	83.157	-3
		0	0	H	2	0	82.204	82.227	$+23$
		1	0	H	3	0	83.007	82.986	-21
8									
		0	0	${}^3D$	0	1	67.686±0.011	67.688	$+2$
		-1	0	${}^1F$	1	0	57.604±0.012	57.602	-2
				${}^3F$	1	0	57.619	57.618	-1
		0	0	${}^1F$	2	0	56.660	57.665	5
				${}^3F$	2	0	56.684	57.688	4
		1	0	${}^1F$	3	0	56.994	56.990	-4
				${}^3F$	3	0	57.026	57.022	-4

TABLE IV. Zero-field energy intervals derived from anticrossing positions.

		This work		Optical
n	Interval	(GHz)	(cm^{-1})	(cm^{-1})
6	^1P-$^1F_3$	373.996±0.015	12.4752±0.0005	12.45
	^1P-H_{av}	363.121±0.018	12.1124±0.0006	
7	^1P-$^1F_3$	237.016±0.032	7.9060±0.0011	7.98
	^1P-H_{av}	229.994±0.050	7.6718±0.0017	
8	^1P-$^1F_3$	159.430±0.017	5.3180±0.0006	5.35

Since this does not affect the line shape except for an overall intensity factor, it is not of great concern.

The most important variable is temperature. Although it is not measured directly, its effect has been well studied in previous work,[2] the results of which can be applied to this case.

In actual practice, the temperature T is taken as a variable to be determined in the line fitting process. However, there are restraints upon allowable values of T. We found that for all ^1P-$^{1,3}F$ signals, the temperature ranged from 280 to 320 K ($\pm\sim 15$ K), whereas for the $n=7$ and 8, ^1P-H signals the T values needed to fit the lines are about 330 to 360 K ($\pm\sim 30$ K) and $n=6$, ~ 380 to 400 K ($\pm\sim 20$ K). This variation is fairly small, and most importantly, the values of the H_0's obtained are unaffected by such variation in T within experimental error. In a recent study[2] of the $9\,^1S$-$9\,^1L$ transition, a considerably larger temperature variation was observed.

B. Zero-field interval determination

The experimental H_0 values, as determined by the line-shape analysis, are listed in Table III along with their estimated errors. The next step in the iterative procedure is to predict the H_0's using the Hamiltonian of Sec. III B. The primary input parameters for this calculation are the zero-field energy separations of the relevant levels. As described earlier, a number of these intervals are fixed at their previously determined values as given in Table II. The two intervals determined by the present data are $n\,^1P_1$-$^1F_3$ and $n\,^1P_1$-H_{av} (the separation between $^1H_3$ and $^3H_3$ being neglected). The values obtained for these intervals, based on a best fit to the observed H_0's, weighted by the square of their estimated errors, are given in Table IV.

Looking at the residuals between the observed and calculated values of the H_0's as given in Table III, one can see that overall the calculated values of the H_0's agree well with the experimental ones, especially considering the possibilities for small systematic errors in the line-shape fitting or small deviations of the Zeeman parameters from their fixed values. (For instance, the diamagnetic Zeeman parameter is calculated using quantum defect corrected radial wave functions only and must be accurate to less than 10% to reproduce the spectrum.)

TABLE V. Measured energy intervals $\Delta\nu$ of $n\,^1P$-$n\,^1D_2$ of ^{4}He. The predicted values of $\Delta\nu$, based upon Eq. (14) and the coefficients given by Table VII are given in column 3.

			$\Delta\nu$	
n	$\Delta\nu_{^1P\text{-}^1D_2}$ (GHz)	Source	Predicted (GHz)	Residual (MHz)
3	3129.7915±0.003	a	3129.7915	0.0
6	423.780 ±0.015	b	423.7765	+3.5
7	268.574 ±0.032	b	268.5796	−5.6
8	180.656 ±0.018	b	180.6656	−9.6
9	127.226 ±0.018	c	127.2409	−14.9
16	22.8080±0.0002	d	22.8069	+1.1
17	19.0215±0.0004	d	19.0213	+0.2
18	16.0294±0.0006	d	16.0289	+0.5

[a] Reference 23.
[b] This work.
[c] Reference 2.
[d] Reference 24.

TABLE VI. G-H intervals in MHz.

n	Present work	Electric field ac[a]	rf beam[b]	Theory[c]
6	2021±23			
7	1318±59	1437±38	1359.16±0.11	1350
8		1011±43	931.34±0.44	900
9	695±64[d]	712±59		630
10		537±85		481

[a] Reference 3.

[b] Reference 4.

[c] Reference 22.

[d] Reference 2.

There are no values listed in Tables III or IV regarding the $8^{1,3}H$ state. This is because the S/N ratio on this data is poor and essentially complete diamagnetic mixing between the H and K states render the analysis with poor data useless.

From the results in Tables II and IV it is possible by simple arithmetic manipulation to derive the $n\,{}^1P$-${}^1D_2$ and $n\,{}^1G_3$-H_{av} intervals. We list these results in Tables V and VI, respectively. From the errors given in Tables V and VI, it is seen that the $n\,{}^1P$-${}^1D_2$ intervals retain errors comparable to the experimental precision, while the $n\,{}^1G_3$-H_{av} interval errors are several times the precision of the measurements. The values for the $n=6,7,8\,{}^1P$-${}^1D_2$ intervals derived in this work are, by at least an order of magnitude, the highest precision results for these intervals.

The same can be said for the $n=7\,{}^1G_3$-${}^1H_{\text{av}}$ interval. For $n=7$, there is a higher precision measurement[4] with which our measurement agrees within its experimental error. From Table IV it can be seen that the anticrossing measurements of Beyer and Kollath[3] constitute the most extensive data set for the $n\,{}^1G$-${}^1H_{\text{av}}$ intervals. However, it should be cautioned that by comparison to our result for $n=8$ and the Cok and Lundeen measurements[4] for $n=7$ and 8, the Beyer and Kollath intervals seem systematically too large by roughly twice their experimental error. Theory[22] also appears to confirm this trend.

C. Power-series representation of the results

In Table V we show our results for the ${}^1P$-${}^1D_2$ intervals and the results of three other precision measurements; a laser measurement for $n=3$,[23] a laser measurement for $n=9$,[2] and microwave measurements for $n=16$, 17, and 18.[24] The uncertainties quoted for those intervals obtained from our anticrossing and laser work include a generous estimate of any possible systematic errors and experimental uncertainties. The uncertainties listed for the other intervals are those quoted by the respective authors.

We have used the data presented in Table V to derive coefficients for the expansion[5]

$$\Delta\nu = A/n^3 + B/n^5 + C/n^7 \,. \tag{14}$$

Such expansions have been shown to be very accurate in predicting all He intervals between any given pair of angular momentum states.[1] Although the ${}^1P$-${}^1D_2$ interval coefficients have been previously determined using microwave and optical data,[24] due to the relative inaccuracy of the optical data and the very high n values of the microwave data, the statistical significance of the previously published B and C coefficients is very low and the possibility of systematic error is significant. Our new values for A, B, and C, which are significantly different from the values obtained by MacAdam and Wing,[24] are given in Table VII along with the one standard deviation error associated with each coefficient. The values of A, B, and C are highly correlated, and we therefore also present their correlation matrix in Table VII.

In deriving the coefficients given in Table VII, we chose to give slightly less significance to the microwave data points than the very small uncertainties quoted by the authors and shown in Table V. The determined intervals all have Stark shift corrections of a few MHz, the accuracy of which are very difficult to determine. In addition, if we use the previously determined[24] A, B, and C coefficients, we predict $n=6$, 7, 8, and 9 intervals that are all systematically greater than the measured values, by as much as 196 MHz for $n=6$ compared to the quoted uncertainty of 15 MHz. By using only our data and

TABLE VII. Correlation matrix for coefficients A, B, and C in Eq. (14) for ${}^1P$-${}^1D_2$ ^{4}He intervals; $A=93\,719.01\pm3.87$, $B=-77\,155.0\pm203$, and $C=-51\,993.5\pm1544$.

	A	B	C
A	1.00	−0.929	0.899
B	−0.929	1.00	−0.997
C	0.899	−0.997	1.00

the $n=3$ interval to derive A, B, and C coefficients we predict intervals for $n=16$, 17, and 18 that are always smaller than the measured values but fall within 3 to 4 MHz of the measurements. In light of these considerations we assigned uncertainties of ± 2.5 MHz to the $n=16$, 17, and 18 intervals in deriving the A, B, and C coefficients of Table VII. The uncertainties used for the other intervals are those listed in Table V.

In fitting the data to the series expansion of Eq. (14) we also attempted to include even power terms such as n^{-4}. The coefficient for such a term turned out to have no statistical significance and did not improve the expansion series modeling of the data. The last two columns of Table V list the predicted values of the intervals based on the coefficients in Table VII and the difference between the measured and predicted values. As can be seen from the very small and reasonable (within experimental uncertainties) residuals, Eq. (14) is a sufficient model to very high accuracy.

---

[*] Present address: Bar Ilan University, Physics Department, Ramat Gam, Israel.

[†] Guest Scientist: Francis Bitter National Magnetic Laboratory.

[1] J. W. Farley, K. B. MacAdam, and W. H. Wing, Phys. Rev. A 20, 1754 (1979), and references therein.

[2] R. Panock, M. Rosenbluh, B. Lax, and T. A. Miller, Phys. Rev. A 22, 1050 (1980), and references therein; M. Rosenbluh, H. Le, B. Lax, R. Panoch, and T. A. Miller, Opt. Lett. 6, 99 (1981).

[3] H. J. Beyer and K. J. Kollath, J. Phys. B 11, 979 (1978).

[4] D. R. Cok and S. R. Lundeen, Phys. Rev. A 23, 2488 (1981).

[5] T. N. Chang and R. T. Poe, Phys. Rev. A 14, 11 (1976).

[6] M. Leventhal, Phys. Lett. 20, 625 (1966).

[7] H. Wieder and T. G. Eck, Phys. Rev. 153, 103 (1967).

[8] G. C. Neumann, B. R. Zegarski, T. A. Miller, M. Rosenbluh, R. Panoch, and B. Lax, Phys. Rev. A 18, 1384 (1978).

[9] An anticrossing mechanism is often difficult to uniquely define. However, this appears to be the only mechanism consistent with the observed selection rules, and rough computation of the magnitude of the perturbing matrix elements is consistent with the anticrossing widths. Finally, the detailed explanation of the line shapes, based upon this mechanism, confirms the correctness of this mechanism.

[10] T. A. Miller and R. S. Freund, Adv. Magn. Reson. 9, 49 (1977).

[11] E. Merzbacher, *Quantum Mechanics* (Wiley, New York, 1970).

[12] H. Le, Ph.D. thesis, MIT, 1982 (unpublished).

[13] W. C. Martin, J. Phys. Chem. Ref. Data 2, 257 (1973).

[14] J. M. Seaton, Proc. Phys. Soc. London 88, 801 (1966).

[15] J. M. Seaton, Proc. Phys. Soc. London 88, 815 (1966).

[16] H. Bethe and E. Salpeter, *Quantum Mechanics of One- and Two-Electron Atoms* (Springer, Berlin, 1957).

[17] T. N. Chang and R. T. Poe, Phys. Rev. A 10, 1981 (1974).

[18] D. Cok and S. R. Lundeen, Phys. Rev. A 19, 1830 (1979), and private communication.

[19] S. A. Lewis, F. M. J. Pichanick, and V. W. Hughes, Phys. Rev. A 2, 86 (1970).

[20] L. C. Green, N. C. Johnson, and E. K. Kal, Astrophys. J. 144, 369 (1966).

[21] R. T. Brown and J. Cortez, Astrophys. J. 176, 267 (1972).

[22] C. Deutsch, Phys. Rev. A 13, 2311 (1976).

[23] A. Javan, *Fundamental and Applied Laser Physics, Proceeding of the Esfahan Symposium*, edited by M. S. Feld, A. Javan, and N. A. Kurnit (Wiley, New York, 1973), p. 307.

[24] K. B. McAdam and W. H. Wing, Phys. Rev. A 13, 2163 (1976).